applied sciences

MDPI

Article

The Reference Phase Correction for the Fluctuated Scanning Lines and the Slope of the Stage in Tissue Characterization by Scanning Acoustic Microscope

Nguyen Thanh Phong Truong [1], Hyehyun Kim [2], Donghae Lee [1], Yeon-Hee Kang [1,3], Sungsoo Na [4] and Junghwan Oh [1,2,5,*]

1 Department of Biomedical Engineering, Pukyong National University, Busan 48513, Korea; phongtruongbk@gmail.com (N.T.P.T.); ldonghae320@gmail.com (D.L.); kyhnuclear@naver.com (Y.-H.K.)
2 Marine-Integrated Bionics Research Center, Pukyong National University, Busan 48513, Korea; hyehyunkim@pknu.ac.kr
3 (BK21 Plus) Marine-Integrated Biomedical Technology Program, Pukyong National University, Busan 48513, Korea
4 Department of Biomedical Engineering, Indiana University-Purdue University Indianapolis, Indianapolis, IN 46202, USA; sungna@iu.edu
5 Ohlabs Corporation, Busan 48513, Korea
* Correspondence: jungoh@pknu.ac.kr; Tel.: +82-51-629-5771; Fax: +82-51-629-5779

Received: 10 September 2019; Accepted: 12 November 2019; Published: 14 November 2019

Abstract: In this study, a new approach was investigated to extract reference phases from the scanning acoustic microscope to calculate the speed of sound when dealing with the slope of the stage and fluctuation of the scanning lines. To capture the slope and the fluctuation pattern, data of the first lines along the horizontal and vertical axes on the stage were used. A corrective function was then utilized to improve the accuracy of reference phase extraction. The method was then corroborated by demonstrating tumor discrimination in mice skin by means of scanning acoustic microscopy (SAM). B16-F10 melanoma cells were used to grow the tumor. Hematoxylin and eosin (H&E) staining was applied for histology characterization of the sample. A comparison of both acoustics and histology was conducted. Phase analysis was performed to examine the effects of both slope and fluctuation. The results showed that our approach significantly improved the tumor detection and accuracy of scanning acoustic microscopy.

Keywords: reference phases; scanning acoustic microscopy; tissue characterization; slope; speed of sound; melanoma cells

1. Introduction

Optical microscopy, together with histology, has long been used to assess the pathology of suspicious regions of tissue. For a histological examination, tissue needs to be prepared through multiple chemical staining procedures to highlight specific target structures before being observed. Normally, several hours to a few days are required to complete the process. Therefore, this requirement of tissue characterization during operation time has been challenged. Furthermore, the tissue usually loses its biological functions after being stained. Several studies were conducted by using elastography as an alternative tissue characterization modality [1–4]. Each of the modalities applies various loading approaches on the sample and result in strain distribution, which is observed by the imaging method. Magnetic resonance elastography (MRE) is sensitive to the magnetic property of the water and fat content of the tissue. MRE can achieve whole-body imaging with high penetration and low spatial resolution. Meanwhile, optical coherence elastography (OCE) can achieve a higher resolution (up to

the diffraction limit of the optical wavelength) and low penetration (about 1 mm). Ultrasound elastography (USE) has been one of the most popular modalities thank to its ability to integrate into ultrasound systems. The USE is mainly divided into three groups: strain imaging methods, shear wave elastography, and B-mode elastography. With externally normal stress applied, the mechanical strain induced along the direction of the mechanical stress is measured (Young's modulus) in strain imaging [5] while shear wave created and propagated in a direction perpendicular to the mechanical stress is measured (shear modulus) in shear wave elastography [6]. Verasonic's research scanner is able to integrate different array transducers from the various manufacturers. The system is widely used in many studies because of its flexibility in sequencing and data processing modification [5,7,8]. B-mode elastography measures the speed of longitudinal waves, which is used to estimate bulk modulus. Each tissue characterization modality has advantages and disadvantages in deployment in clinical applications and also plays a different role in filling the gap in terms of spatial resolution among them. Among the elastography modalities, B-mode elastography, using a single element transducer, has been utilized for tissue characterization on a microscale owing to its high spatial resolution and simplicity. Due to the correlation of elasticity and speed of sound in the tissue [9], the acoustic velocity of longitudinal waves has been considered to be a parameter for tissue characterization. The single element transducer scans the area of interest of the sample to achieve two-dimensional sound-speed images. Several authors have reported the use of scanning acoustic microscopy (SAM) for the tissue characterization of various anatomical regions [10–15].

During the early stages of tissue characterization by SAM, several studies have calculated acoustic velocity [16–18]. In histology and pathology, thin slices of tissue from about several micrometers to several tens of micrometers thick were used for characterization. The interferential method has been the most popular method, where the distance between two reflections at the tissue is under one wavelength. In this method, the phases of the two reflections are compared with the reference phases, which are determined from the substrate without the tissue. The reference phases are identical at every position if the substrate surface and scanning line of the transducer are parallel.

However, determining the reference phases has been a challenge, due to the slope of the scanning stage. There have been numerous attempts to solve this problem [19]. The plane function has been widely used in previous studies. In this method, the slope of the stage on each axis was compensated by the time lags among three points without the tissue [20,21]. The plane function is useful, if the scanning lines obtained from both motors are flat.

However, in real applications, the systematic errors of the shaft of the motor and its aging could result in the fluctuation of the scanning lines. When the automate factor is included, the slope of the scanning line needs to be considered. The combination of the slope of the stage and the fluctuation of the scanning line of the motors could result in unstable reference phase extraction.

In this study, we built a system that could change the fluctuation of the scanning line of the motors and the slope of the stage. The changeable factors create different situations for the study. A new approach used data of the first lines along the horizontal axis (X axis) and vertical axis (Y axis), where no tissue is present, to capture both the slope and the fluctuation pattern. To minimize the effects, the corrective function was finally applied.

To validate our approach, tumor discrimination using mice skin was conducted. Melanoma cells were used to grow the tumor. After characterization by SAM, the sample was stained by Hematoxylin and eosin (H&E) for histological observation. A comparison of acoustic and histological characterization was carried out.

2. Materials and Methods

2.1. Hypothetical Calculation

Elasticity is determined by relating force to deformation, which is called the elastic modulus. All materials can be depicted in terms of elastic modulus. Elasticity reflects the ability of an object to

resist a deformation force and return to the original size when the force is removed. Elastic modulus can be described as:

$$Elastic\_\text{modulus} = \frac{Stress}{Strain} = \frac{Force/Area}{Change\_in\_length/Original\_length}, \quad (1)$$

The speed of sound and elasticity are related closely by the following equation:

$$c = \sqrt{\frac{E}{\rho}}, \quad (2)$$

where c, E, ρ is the speed of sound in the object, the elastic modulus of the object, and density of the object, respectively. Note that Equation (1) is a general rule to estimate the elasticity of an object when an external force is applied. The Equation (2) shows the relation between acoustic velocity and an elastic modulus. Depending on how the force is applied to the object, the appropriate elastic modulus (Young, shear, bulk moduli) would be considered in the calculation.

To calculate the speed of sound of a thin layer where one reflection overlaps another, a phase comparison between the reflections was conducted.

Figure 1 demonstrates the phase values at the top and bottom of the sample in comparison with the phase at the surface of the substrate. Here, a single ultrasonic frequency is considered. The practical signal is composed of several frequencies that mostly depend on transducer characteristics. The reflective signal from the tissue is the sum of two reflections at the front side and the back side of the tissue. The calculation relies on the interference of reflections determined by the acoustic properties of the tissue. The destructive interference is used for the calculation. Then, the phase difference between the front and the back surfaces of the tissue will be multiple odd numbers of 180 degrees. In other words, the two reflections would be out of phase. The relation of the phase values at the surfaces is detailed in Equations (3) and (4). The explanation for the destructive interference of the two reflections is shown in Figure 2 in the case of n = 1.

$$\phi_s = \phi_m + (2n-1)\pi = 2\pi f_m \frac{2d}{c_0}, \quad (3)$$

$$\phi_d = \phi_m = 2\pi f_m \left(\frac{2d}{c_0} - \frac{2d}{c}\right), \quad (4)$$

where c_0, c, and d, are the speed of sound in water, the speed of sound in tissue, and the thickness of tissue, respectively. ϕ_s is the phase at the front side of the tissue, and ϕ_d is the phase at the back side of the tissue. f_m is the frequency that induces the interference, and ϕ_m is the corresponding phase of the frequency.

$$d = \left\{\phi_m - \phi_{ref} + (2n-1)\pi\right\}\frac{c_0}{4\pi f_m}, \quad (5)$$

$$c = \left(\frac{1}{c_0} - \frac{\phi_m - \phi_{ref}}{4\pi f_m d}\right)^{-1}, \quad (6)$$

Equations (5) and (6) show how the thickness and speed of sound of a specific point are calculated. Equations (5) and (6) are derived from Equations (3) and (4) with compensation to the reference phase ϕ_{ref}.

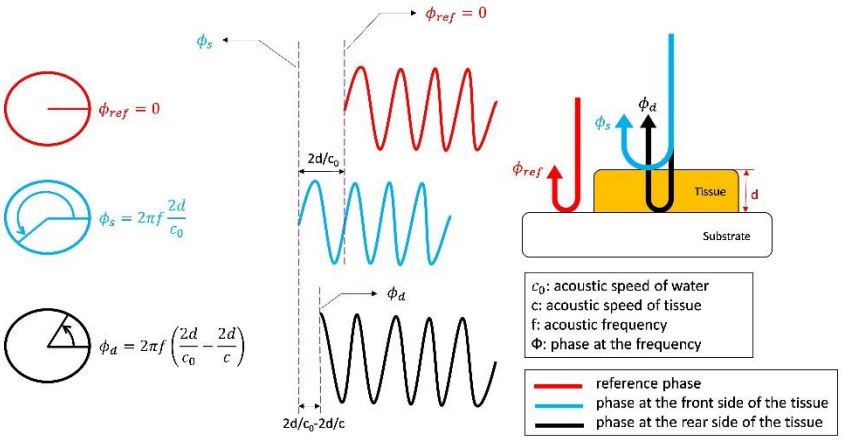

Figure 1. Phase distribution over the sample. ϕ_d is the phase at the back side of the tissue. ϕ_s is the phase at the front side of the tissue. ϕ_{ref} is the phase at the surface of the substrate, d is the thickness of the tissue.

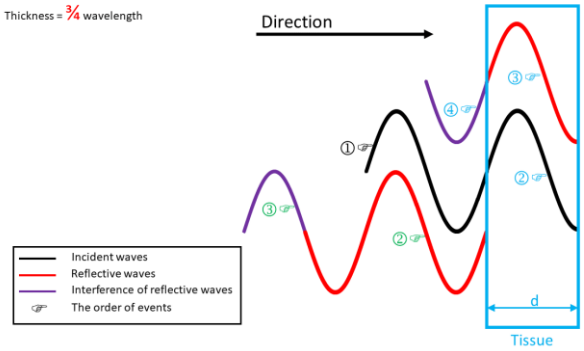

Figure 2. Interference reflections of tissue. The acoustic waves approach from the front side (as the direction arrow) of the tissue with thickness d. The event marked in black presents the incident waves. The event marked in blue belongs to the transmission part. The event marked in green belongs to the reflection part.

Figure 2 visually explains that the destructive interference in the tissue thickness is equal to three-fourths of the wavelength in the tissue. In this example, phase reversion is ignored when an acoustic wave is reflected from the higher acoustic impedance medium. Initially, the incident wave from the transducer hits the front side of the tissue. At the front surface, the wave breaks into two parts (the transmission part marked in blue and the reflection part marked in green in Figure 2) because of the impedance differences between the two media. The transmission part keeps traveling inside the tissue; it reflects back when it approaches the rear side and then exits from the tissue. Depending on tissue characteristics, such as thickness (travel distance) and speed of sound, the transmitted part of the wave that exits the tissue is out of phase with the reflected part of the wave. As a result, the exiting wave and the reflection part interfere destructively with each other.

2.2. Experimental Setup

Figure 3 is a rendering image of the SAM system (Ohlabs Co., Busan, Korea) used in this study. The system consists of three main parts: the slope adjustment stage (Figure S1), an integrated microscope (Figure S2), and a pair of X–Y linear scanning motors (Figure S3). The stage was built on three post holders. Whereas one post holder was stationary, the other two posts were able to translate along its vertical axis. The function of the translating post holder was to regulate the slope of the stage along the X–Y direction in accordance with each post holder's position. The upper motor that the transducer compact was mounted on was used as a scanning motor. The shaft of the lower motor that

was purposely modified to make it significantly rough was used as an advance motor. The rough shaft of the motor was used to create the random fluctuation of the scanning lines for the study. The motors were originally manufactured by Newport and controlled by a three-axis motion controller (ESP301, Newport, Irvine, CA, USA). The transducer was scanned following a zig-zag pattern. A 60-MHz central frequency transducer (Olympus, Tokyo, Japan) was used in this study. The transducer was operated in echo mode. The detected signal was introduced into a digitizer (PXI-5152, National Instruments, Austin, TX, USA) at a sampling rate of 2 GS/s. The program in the study was self-made by using Labview (Labview 2014, National Instruments, Austin, TX, USA). Most of the mechanical components were manufactured by Thorlabs (Newton, NJ, USA). The room temperature was maintained at 25 °C. The speed of sound in water was measured at each scanning to increase the accuracy. To reduce the random noise, five response times at one data point were averaged.

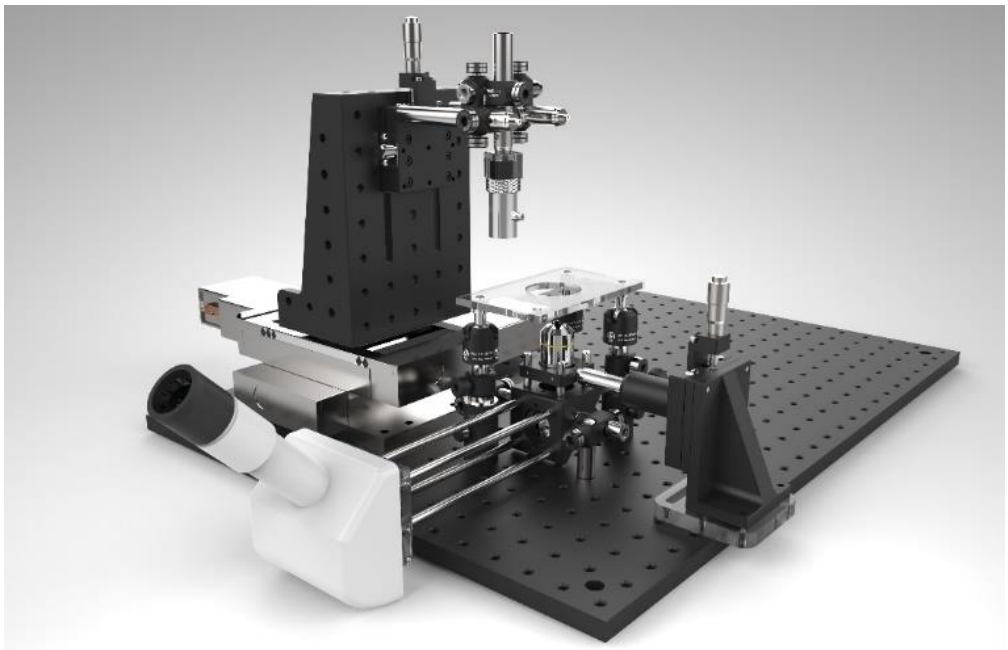

Figure 3. Scanning acoustic microscope (SAM) system.

2.3. Tissue Preparation

To study the biopsy application of tissues by the SAM system, a B16-F10 melanoma cell line was purchased from the Korean Cell Line Bank (Seoul, Korea). Cells were cultured in Dulbecco's modified Eagle's medium (DMEM; Hyclone), supplemented with 10% fetal bovine serum (FBS) and antibiotics (1% penicillin/streptomycin) in the atmosphere at 37 °C under 5% CO_2. Female BALB/c nude mice (6–7 weeks old) were purchased from Orient Bio Inc. (Seongnam, Korea). B16-F10 melanoma cells (1×10^6 cells) suspended in 100 μL of phosphate buffered saline (PBS) were injected subcutaneously into the flanks of each mice. The cancer cells were allowed to proliferate and spread over a 100–150 mm^3 area on the mice skin. The paraffin block method was adopted to prepare a biopsy tissue specimen. A 20 μm paraffin section was prepared by Leica Biosystems RM2245 Semi-Automated Rotary Microtome (Leica Inc., New Jersey, USA) and placed on the positively charged slide. Prior to the scanning experiment by the SAM system, the samples were treated with Xylene to remove paraffin. The tissue processing is graphed in Figure S4.

2.4. Practical Calculation

The f_m, ϕ_m, and, ϕ_{ref} values of each point were required to calculate the thickness and speed of sound of the samples. After the analog-digital converter, a Fast Fourier transform (FFT) of the signal

(A-scan) was computed. The product of FFT was a complex number. The real and imaginary parts contained frequency and phase information, respectively.

The interference of the two reflections (front and back sides of tissue) occurred at frequency f_m in condition [22]:

$$f_m = \frac{nc}{2d}, \ (\mathrm{n} = 0,\ 1,\ 2,\ 3\ldots) \tag{7}$$

where f_m, c, d are the frequency that induces the interference, speed of sound in tissue and thickness of the tissue, respectively. The Equation (7) can assist the work in approximating the interference frequency when acoustic velocity and thickness are in a known range of values.

Figure 4c shows that the magnitude (peak to peak) of the first reflection from the front side of the tissue is about 10% of the rear one. Consequently, obtaining the interferential frequency from the spectrum in Figure 4d was difficult. Therefore, the spectrum in Figure 4d was normalized by the reference spectrum in Figure 4b, which resulted in Figure 4e. The reference spectrum in Figure 4b was the product of FFT from the signal in Figure 4a, which was reflected from the substrate. The interferential frequency (f_m) was obtained from the nominal spectrum in Figure 4e. According to the derived frequency (f_m), its phase value (ϕ_m) was determined in Figure 4f. The reference phase ϕ_{ref} is the phase of the signal that reflected directly from the substrate at the calculating point. As a result, the reference phase at the calculating point was indirectly calculated owing to tissue coverage at this point. The determination of ϕ_{ref} are mentioned below. Finally, the thickness and speed of sound of the point were determined by replacing f_m, ϕ_m, and ϕ_{ref} in Equations (5) and (6). The acoustic velocity of water coupling was measured by the time lag between two specific points when translating the transducer along the Z-axis. The transducer was scanned over the region of interest. Each point of the sample was calculated to create 2D images.

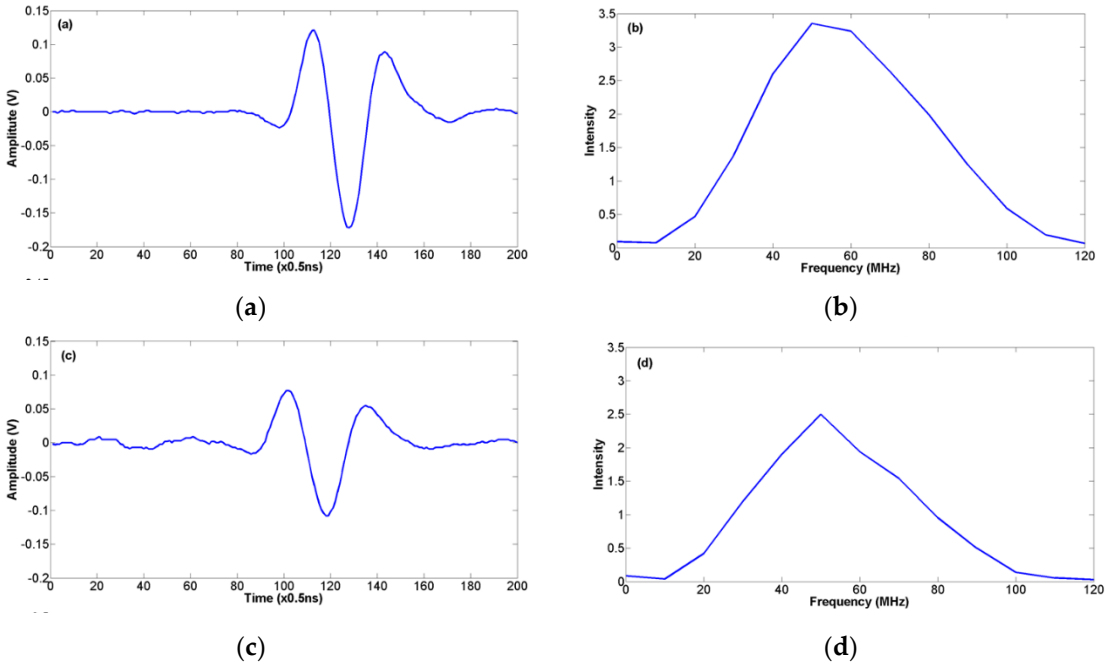

Figure 4. *Cont.*

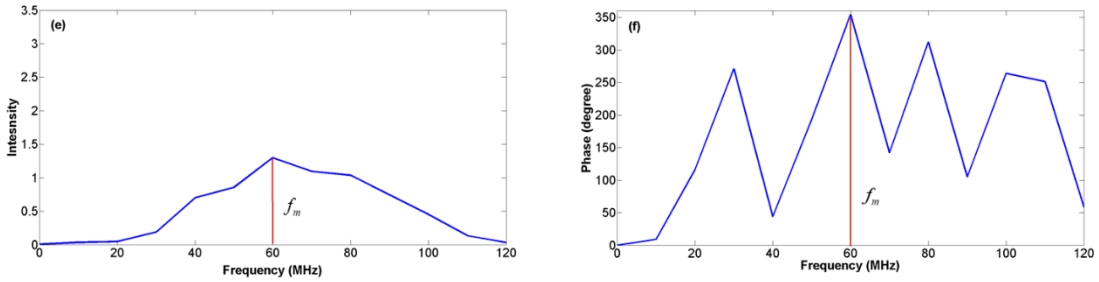

(**e**) (**f**)

Figure 4. Example of waveforms for calculation: (**a**) A-scan signal reflected from the substrate; (**b**) Spectrum of (a) after FFT; (**c**) A-scan reflected from the tissue; (**d**) Spectrum of (c); (**e**) Nominal spectrum of (d) and (b); (**f**) Corresponding phase of (d).

In this study, the mice skin containing the tumor region were used as the sample for scanning. We proposed a method that used data of the first vertical line (Y axis) and the first horizontal line (X axis) to detect the slope of the stage and the fluctuation pattern shown in Figure 5a,b. The slope of the stage was controlled by the slope adjustment stage, and the fluctuation was determined by the shaft of the motors. For this reason, the first vertical and horizontal lines (along Y and X axes, respectively) need to be reserved in empty (without tissue) as a setup condition, which is described in Figure 5d.

Figure 5a,b are the graphs of the phase values at 60 MHz along the Y and X axes, respectively. The red straight lines in the graphs connecting the beginning point and the ending point demonstrate the mismatch between the fluctuated situation and plane function in terms of reference phase extraction. The X-axis was used for scanning and the Y-axis was used for advancing. Figure 5a demonstrates the significant fluctuation and slope of the stage along the Y-axis. The slope of the stage is intentionally regulated as a setup condition for this experiment. Figure 5c is the 2D acoustic velocity image using plane function. In such cases of slope and fluctuation, the plane function gives unreliable results.

Previous studies have determined the reference phases by using the plane function. These studies were performed by obtaining the phase values at three corners of the scanning area. Then, the plane function was built, and the reference phase was extracted from this function to compensate for the slope of the scanning stage.

In this study, we developed a function that improves the accuracy of reference phase extraction in case the scanning is fluctuating:

$$\phi_{ref}(x, y, f) = \phi_{y0}(x, f) + \phi_{x0}(y, f) - \phi_{x0}(0, f), \tag{8}$$

where ϕ_{y0} and ϕ_{x0} are the phase functions of frequency f of the first horizontal line and the first vertical line, respectively.

Equation (8) returned the reference phase of positions in the scanning area by the selected frequency f and its coordinates (x and y). The frequency was the interferential frequency of a calculating point. The equation was derived by tracing the repeated phase changes on the scanning axis $\phi_{y0}(x, f)$ (based on phase values on the first horizontal line) and compensating the phase change on the advance axis $\phi_{x0}(y, f) - \phi_{x0}(0, f)$ (based on phase values on the first vertical line). The compensation on the advance axis was conducted by comparing the phase change between the calculating point $\phi_{x0}(y, f)$ and the beginning point $\phi_{x0}(0, f)$ of the vertical axis. In other words, when the phase changed on the advance axis because of fluctuation and slope, it changed the overall phase on the scanning axis. As a result, the phase change on the scanning axis maintained the same pattern but reduced the amount of the advance axis's change. By determining the amount of change on the advance axis $\phi_{x0}(y, f) - \phi_{x0}(0, f)$, the phase change on the scanning axis was compensated. Consequently, the reference phase extraction of every position was improved by taking the phase change compensation of both axes into consideration.

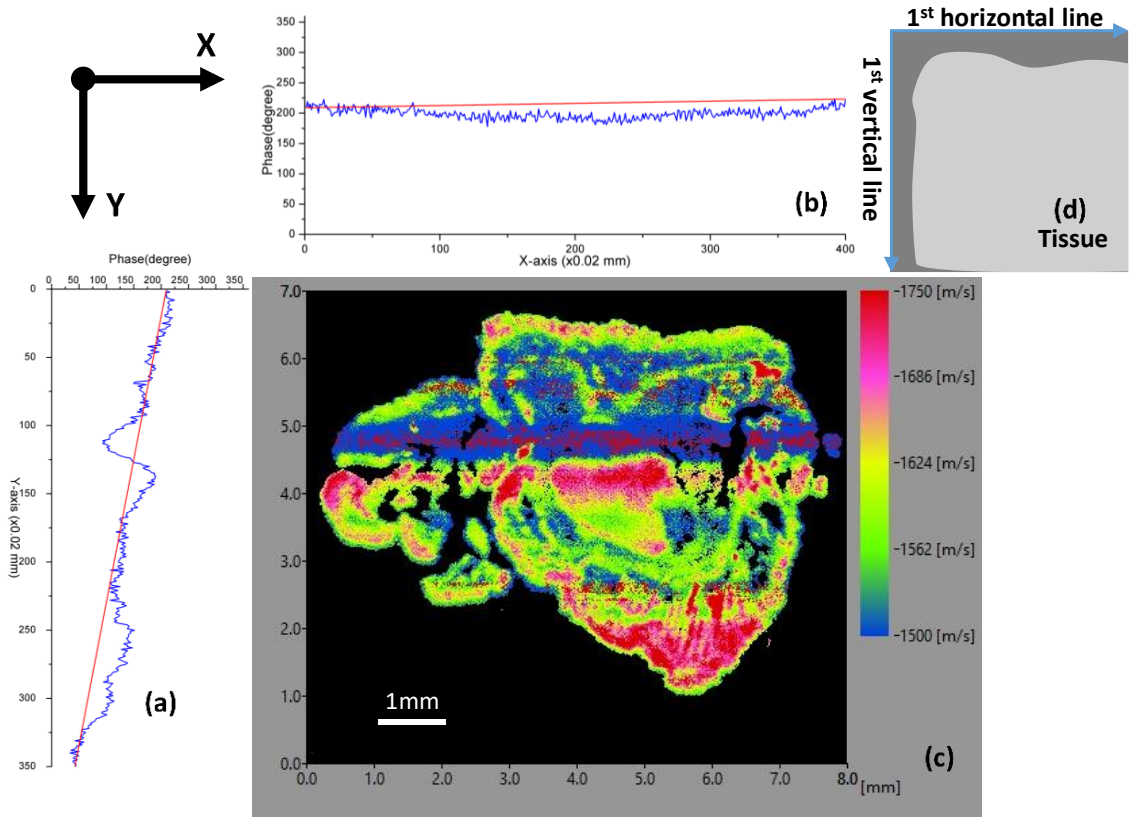

Figure 5. Phase analysis at the first vertical line and the first horizontal line: (**a**) Phase graphs of the first vertical line; (**b**) Phase graphs of the first horizontal line; (**c**) Speed-of-sound image; (**d**) Illustration of the sample setup with the first horizontal and the first vertical lines.

2.5. Statistical Analysis

Data were expressed as the mean ± SD (n = 3) and analyzed using one-way analysis of variance. In all tests, $P < 0.05$ and $P < 0.01$ were regarded as statistically significant.

3. Results and Discussion

The mice skin containing the tumor region were imaged by the SAM system. The reference phase values were corrected and then compared with the H&E stained image, which is shown in Figure 6. The speed-of-sound properties were measured to distinguish between healthy regions and cancerous tissues. Figure 6 also depicts the microscopic image of H&E stained malignant melanoma and surrounding normal tissues, and their corresponding SAM images, mapped from speed-of-sound values, are displayed. Tissues with cell-rich structures such as follicles, malignant melanoma and epidermis demonstrated higher speed-of-sound values than cell-poor structures such as the hypodermis and dermis tissue. The average values of acoustic velocity from different regions are demonstrated in Table 1 and Figure S5. Similar results have been suggested by Youssef et al. [23], indicating that the melanoma cells demonstrate the lowest values of sound speed (1360 ± 50 m/s).

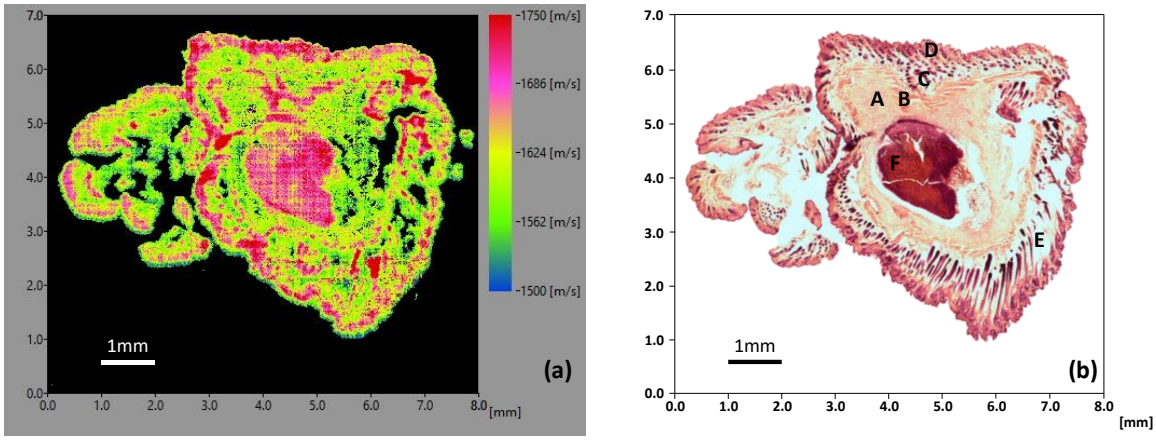

Figure 6. Comparison of the profile of (**a**) acoustic velocity and (**b**) hematoxylin and eosin (H&E) staining. A (upper left) "Dermis" and C (upper middle) "Hypodermis" show lower speed of sound values than B (middle) "Muscle". "Epidermis" (D) and "Back skin layer follicle" (E) have similar high speed-of-sound values. "Malignant melanoma" (F) clearly displays relatively higher scanning acoustic microscopy (SAM) than the surrounding normal tissue.

Table 1. Average speed of sound.

Tissue Skin Layer	Average Speed of Sound (m/s)
Epidermis (D)	1704 ± 43
Hypodermis (C)	1572 ± 17
Muscle (B)	1727 ± 58
Dermis (A)	1595 ± 28
Back skin layer follicle (E)	1693 ± 39
Malignant melanoma (F)	1719 ± 36

In our imaging study depicted in Figure 6a, each skin tissue was distinguished from surrounding tissues by their different acoustic velocities. In Figure 6b, the areas of malignant melanoma were preferably stained with hematoxylin because of the downregulation of intercellular gap junctions between cancerous cells [24]. The speed-of-sound image in Figure 6a agrees with the microscopic H&E stained image in Figure 6b by exhibiting higher acoustic velocity values.

The result in Figure 5c showed a poor correlation with H&E staining in Figure 6b in detecting the cancerous region. The speed of sound in Figure 5c differs from Figure 6a at the location where the reference phase from the plane function and the correction function are different. The magnitude of differences in speed-of-sound value could be explained by Equations 5 and 6. The higher the reference phase extracted from the plane function over the acquired value (in Figure 5a,b), the smaller the value of acoustic velocity in Figure 5c over Figure 6a, and vice versa. This indicates that the accuracy of reference phase extraction in such circumstances plays a crucial role in the result.

As tissue characterization by SAM has been developed for a long time, the problems mentioned in the study (slope and fluctuation of the scanning lines) may be solved by hiding techniques or they have been worked around when facing the problems (by replacing a new motor). By taking the practical factors of slope and fluctuation into account, this study could be one step further to improve the accuracy of SAM. With our approach, the corrective function works in cases of the slope of the stage, with and without the fluctuation of the scanning lines.

In this study, other noise sources, such as phase noise (called jitter caused by unideal oscillating clocks on the electrical devices) of the digitizer, and the inhomogeneous responses of the transducer, were considered as random noises. The noises could cause fluctuations in the phase of the measured signal. The fluctuations were reduced by averaging five times the sampling of each data point. Table S1 and Figure S6 show the differences of random noise at different frequencies and graphs of the values, respectively. The phase values sampled at frequencies 33 MHz and 88 MHz according to the boundary

response of the transducer. Based on Equations (5) and (6), the effects of the random noise on phases cause the change of acoustic velocity could be estimated as:

$$\Delta c = \frac{c_0}{3\pi}\Delta\phi, \tag{9}$$

where $\Delta\phi$ is the phase change by random noise causes the change in acoustic velocity Δc. By Equation (9) and the data in the Table S1, the random noise has minor effects on the result compared with the fluctuations from the scanning lines.

Although tumor discrimination in this study was testified by a high percentage of matching between speed-of-sound and H&E staining images, higher resolution of the transducer is needed for smaller structure studies.

Tissue characterization by SAM could potentially be utilized in practice, where it could work alternatively with conventional histology methods. In order to deploy it completely in the field, where a variety of factors could affect the results, SAM for tissue characterization need to be more robust.

4. Conclusions

The nonlinear slope stage can cause inaccuracy of the SAM system, and using plane function to compensate the slope may not be an appropriate method to correct the problem. The proposed method improved the accuracy of the system, exhibiting the fluctuated scanning lines and the slope of the stage. We applied this new method to visualize the speed of sound of the mice skin and compared the result with the histology image. In the acoustic image, the average value of the tumor region (1719 m/s ± 36) was slightly higher than that of the epidermis (1704 m/s ± 43) and back skin layer follicle regions (1693 m/s ± 39). In the comparison of Figures 5c and 6a, our approach significantly improved the scanning accuracy.

Supplementary Materials: The following are available online at http://www.mdpi.com/2076-3417/9/22/4883/s1, Figure S1: The slope adjustment stage, Figure S2: The integrated microscope part of the system, Figure S3: A pair of linear scanning motor, Figure S4: Schematic illustration of tissue processing, Figure S5: Average speed of sound, Figure S6: Graphs of the phase values from Table S1, Table S1: The typical values of phase caused by random noise

Author Contributions: N.T.P.T. wrote the main manuscript text and made the computed program. H.K. and D.L. and Y.-H.K. prepared tissue samples and conducted experiments. S.N. and J.O. managed workflow and gave instructions. All authors reviewed the manuscript.

Acknowledgments: This work was supported by a grant from the Marine Biotechnology Program (20150220) funded by the Ministry of Oceans and Fisheries, Korea.

Conflicts of Interest: The authors declare no conflict of interest.

References

1. Manduca, A.; Oliphant, T.E.; Dresner, M.A.; Mahowald, J.L.; Kruse, S.A.; Amromin, E.; Felmlee, J.P.; Greenleaf, J.F.; Ehman, R.L. Magnetic Resonance Elastography: Non-Invasive Mapping of Tissue Elasticity. *Med. Image Anal.* **2001**, *5*, 237–254. [CrossRef]
2. Wang, S.; Larin, K.V. Optical Coherence Elastography for Tissue Characterization: A Review. *J. Biophotonics* **2014**, *8*, 279–302. [CrossRef] [PubMed]
3. Sigrist, R.M.; Liau, J.; El Kaffas, A.; Chammas, M.C.; Willmann, J.K. Ultrasound Elastography: Review of Techniques and Clinical Applications. *Theranostics* **2017**, *7*, 1303–1329. [CrossRef] [PubMed]
4. Garra, B.S. Elastography: History, Principles, and Technique Comparison. *Abdom. Imaging* **2015**, *40*, 680–697. [CrossRef]
5. Patel, V.; Dahl, J.J.; Bradway, D.P.; Doherty, J.R.; Smith, S.W. Acoustic Radiation Force Impulse Imaging on an IVUS Circular Array. In Proceedings of the 2013 IEEE International Ultrasonics Symposium (IUS), Prague, Czech Republic, 21–25 July 2013. [CrossRef]
6. Taljanovic, M.S.; Gimber, L.H.; Becker, G.W.; Latt, L.D.; Klauser, A.S.; Melville, D.M.; Gao, L.; Witte, R.S. Shear-Wave Elastography: Basic Physics and Musculoskeletal Applications. *RadioGraphics* **2017**, *37*, 855–870. [CrossRef]

7. Song, P.; Zhao, H.; Urban, M.W.; Manduca, A.; Pislaru, S.V.; Kinnick, R.R.; Pislaru, C.; Greenleaf, J.F.; Chen, S. Improved Shear Wave Motion Detection Using Pulse-Inversion Harmonic Imaging with a Phased Array Transducer. *IEEE Trans. Med. Imaging* **2013**, *32*, 2299–2310. [CrossRef]
8. Hansen, H.H.G.; Saris, A.E.C.M.; Vaka, N.R.; Nillesen, M.M.; De Korte, C.L. Ultrafast Vascular Strain Compounding Using Plane Wave Transmission. *J. Biomech.* **2014**, *47*, 815–823. [CrossRef]
9. Saijo, Y. Acoustic Microscopy: Latest Developments and Applications. *Imaging Med.* **2009**, *1*, 47–63. [CrossRef]
10. Saijo, Y.; Miyakawa, T.; Sasaki, H.; Tanaka, M.; Nitta, S.I. Acoustic Properties of Aortic Aneurysm Obtained with Scanning Acoustic Microscopy. *Ultrasonics* **2004**, *42*, 695–698. [CrossRef]
11. Miura, K.; Egawa, Y.; Moriki, T.; Mineta, H.; Harada, H.; Baba, S.; Yamamoto, S. Microscopic Observation of Chemical Modification in Sections Using Scanning Acoustic Microscopy. *Pathol. Int.* **2015**, *65*, 355–366. [CrossRef]
12. Saijo, Y.; Tanaka, M.; Okawai, H.; Sasaki, H.; Nitta, S.I.; Dunn, F. Ultrasonic Tissue Characterization of Infarcted Myocardium by Scanning Acoustic Microscopy. *Ultrasound Med. Biol.* **1997**, *23*, 77–85. [CrossRef]
13. Saijo, Y.; Santos Filho, E.; Sasaki, H.; Yambe, T.; Tanaka, M.; Hozumi, N.; Kobayashi, K.; Okada, N. Ultrasonic Tissue Characterization of Atherosclerosis by a Speed-of-Sound Microscanning System. *IEEE Trans. Ultrason. Ferroelectr. Freq. Control* **2007**, *54*, 1571–1577. [CrossRef] [PubMed]
14. Miura, K.; Nasu, H.; Yamamoto, S. Scanning Acoustic Microscopy for Characterization of Neoplastic and Inflammatory Lesions of Lymph Nodes. *Sci. Rep.* **2013**, *3*. [CrossRef] [PubMed]
15. Bilen, B.; Sener, L.T.; Albeniz, I.; Sezen, M.; Unlu, M.B.; Ugurlucan, M. Determination of Ultrastructural Properties of Human Carotid Atherosclerotic Plaques by Scanning Acoustic Microscopy, Micro-Computer Tomography, Scanning Electron Microscopy and Energy Dispersive X-ray Spectroscopy. *Sci. Rep.* **2019**, *9*. [CrossRef] [PubMed]
16. Okawai, H.; Tanaka, M.; Dunn, F. Non-Contact Acoustic Method for the Simultaneous Measurement of Thickness and Acoustic Properties of Biological Tissues. *Ultrasonics* **1990**, *28*, 401–410. [CrossRef]
17. Saijo, Y.; Tanaka, M.; Okawai, H.; Dunn, F. The Ultrasonic Properties of Gastric Cancer Tissues Obtained with a Scanning Acoustic Microscope System. *Ultrasound Med. Biol.* **1991**, *17*, 709–714. [CrossRef]
18. Van der Steen, A.F.W.; Cuypers, M.H.M.; Thijssen, J.M.; De Wilde, P.C.M. Influence of Histochemical Preparation on Acoustic Parameters of Liver Tissue: A 5-MHz Study. *Ultrasound Med. Biol.* **1991**, *17*, 879–891. [CrossRef]
19. Lee, C.K.; Murakami, Y.; Hozumi, N.; Nagao, M.; Kobayashi, K.; Saijo, Y.; Tanaka, N.; Ohtsuki, S. Improvement of the Precision of Ultrasonic Microscope for Biological Tissue Using the Automatic Extraction of the Reference Signals. *IEEE Trans. Fundam. Mater.* **2005**, *125*, 145–152. [CrossRef]
20. Hozumi, N.; Yamashita, R.; Lee, C.K.; Nagao, M.; Kobayashi, K.; Saijo, Y.; Tanaka, M.; Tanaka, N.; Ohtsuki, S. Ultrasonic Sound Speed Microscope for Biological Tissue Characterization Driven by Nanosecond Pulse. *Acoust. Sci. Technol.* **2003**, *24*, 386–390. [CrossRef]
21. Hozumi, N.; Yamashita, R.; Lee, C.K.; Nagao, M.; Kobayashi, K.; Saijo, Y.; Tanaka, M.; Tanaka, N.; Ohtsuki, S. Time–frequency Analysis for Pulse Driven Ultrasonic Microscopy for Biological Tissue Characterization. *Ultrasonics* **2004**, *42*, 717–722. [CrossRef]
22. Yan, H.; Peng, K.; Xu, C.; Lin, Q. Properties of Copper Film Characterized by Scanning Acoustic Microscope. In Proceedings of the 2013 Far East Forum on Nondestructive Evaluation/Testing: New Technology and Application, Jinan, China, 17–20 June 2013. [CrossRef]
23. Youssef, S.; Seviaryna, I.; Shum, D.; Maeva, E.; Malyarenko, E.; Rahman, N.; Maev, R.G. High-resolution Quantitative Acoustic Microscopy of Cutaneous Carcinoma and Melanoma: Comparison with Histology. *Skin Res. Technol.* **2019**, *25*, 662–671. [CrossRef] [PubMed]
24. Leithe, E.; Sirnes, S.; Omori, Y.; Rivedal, E. Downregulation of Gap Junctions in Cancer Cells. *Crit. Rev.™ Oncog.* **2006**, *12*, 225–256. [CrossRef] [PubMed]